JOURNAL OF CATALYSIS 93, 38–54 (1985)

Temperature-Programmed Reduction of CoO/Al_2O_3 Catalysts

P. ARNOLDY[1] AND J. A. MOULIJN

Institute for Chemical Technology, University of Amsterdam, Nieuwe Achtergracht 166, 1018 WV Amsterdam, The Netherlands

Received October 21, 1983; revised June 5, 1984

It is shown that temperature-programmed reduction (TPR) is a sensitive technique for the characterization of Co– and Co–Al-oxidic phases in CoO/Al_2O_3 catalysts. Four different reduction regions can be present for CoO/Al_2O_3 catalysts, which are assigned to four Co phases (I, II, III, and IV). Phase I (reduction at ca. 600 K in TPR at 10 K/min) consists of Co_3O_4 crystallites. Phase II (reduction at ca. 750 K) consists of Co^{3+} ions, in crystallites of proposed stoichiometry Co_3AlO_6 or in well-dispersed surface species. Phase III (reduction at ca. 900 K) consists of surface Co^{2+} ions. Phase IV (reduction at ca. 1150 K) consists either of surface Co^{2+} ions (with more Al^{3+} ions in their surrounding than in phase III) or of subsurface Co^{2+} ions, occurring in diluted Co^{2+}–Al^{3+} spinel structures or in $CoAl_2O_4$. Al^{3+} ions influence the reducibility of Co ions strongly. This is explained by polarization of Co–O bonds by Al^{3+} ions. Preparation conditions (calcination flow rate and calcination temperature) influence the structure of CoO/Al_2O_3, namely the Co valency, the extent of solid-state diffusion, and the dispersion. Solid-state diffusion of Co^{2+} and Al^{3+} ions occurs above ca. 800 K. The implications of this study for $CoO–MoO_3/Al_2O_3$ hydrodesulfurization catalysts are discussed.

INTRODUCTION

The role of Co in HDS catalysis. Co atoms supported on Al_2O_3 play an important role in catalysis. Very common is the application of Co in $CoO–MoO_3/Al_2O_3$ hydrodesulfurization (HDS) catalysts. This bimetallic catalyst is an order of magnitude more active in HDS than MoO_3/Al_2O_3 or CoO/Al_2O_3 (*1, 2*). Many articles have been published on these catalysts and have treated the question of the relation between HDS activity and structural features (*3–6*). The Mo part of the system is understood reasonably well, but the precise role of Co and the interaction of Co and Mo in HDS catalysis are still uncertain.

Co might have a promoter function by increasing the activity of the Mo component, as assumed in the synergism model (*7*), the pseudointercalation model (*8, 9*), and several other models (*3*). Co might also be equivalent to Mo in the generation of HDS activity, as proposed in the Co–Mo–S phase model (*2, 10*). But Co itself can also have high HDS activity, as has been shown for Co on carbon supports (*11, 12*). For Al_2O_3-supported Co also HDS activity has been reported, which, in some cases, is comparable with the HDS activity of Al_2O_3-supported Mo, if the activity is calculated per mole of metal atoms (*1*). In contradistinction with most literature, we suggest that the high activity of $CoO–MoO_3/Al_2O_3$ might be attributed to Co atoms. In this case Mo might be the "promoter," e.g., by dispersing the active Co phase on the surface (*13*).

The structure of supported Co oxides. In fact it is not possible to draw definite conclusions from the literature on the structure of $CoO–MoO_3/Al_2O_3$. It is remarkable that so many results have been reported on MoO_3/Al_2O_3 and $CoO–MoO_3/Al_2O_3$, whereas reports on the structure of CoO/Al_2O_3 are relatively scarce (*3*).

In most studies it is concluded that in CoO/Al_2O_3 two phases can be present, viz. a crystalline "β-phase" and a dispersed "δ-phase" (*3, 13–23*). The δ-phase predomi-

[1] Present address: Koninklijke/Shell-Laboratorium Badhuisweg 3, 1031 CM Amsterdam, The Netherlands.

0021-9517/85 $3.00

nates at low Co loadings (below ca. 2% CoO), while the β-phase occurs only at higher loadings (up from ca. 2% CoO). The δ-phase consists of Co^{2+} ions dispersed in surface layers of the Al_2O_3 support. This phase shows many spectroscopic and chemical features which are characteristic for bulk $CoAl_2O_4$. It is concluded that these Co ions are "nonreducible" (*17, 18, 20, 24, 25*) and "nonsulfidable" (*17, 20, 26*). The distribution of Co^{2+} ions of the δ-phase over tetrahedral and octahedral positions appears to be a matter of controversy (*3, 13–17, 21, 23, 27*). It is concluded that the β-phase consists of Co_3O_4 crystallites, which can be reduced and sulfided easily. In all cases where Co^{3+} ions were observed their presence was associated with Co_3O_4 formation.

Recently it has been suggested that a third oxidic Co phase is present in CoO/Al_2O_3, on the basis of sulfidability studies (*26*). It is concluded to be nonreducible like the δ-phase, but discernible from the δ-phase by being sulfidable. Also in the presence of Mo, in $CoO–MoO_3/Al_2O_3$, three Co phases have been detected in the sulfided state (*10, 21, 26, 28*). Besides Co_9S_8, resulting from Co_3O_4 crystallites, and nonsulfidable Co^{2+} ions in the oxidic Al_2O_3 lattice (δ-phase), a third, sulfided, Co species has been found, referred to as Co–Mo–S (*10*) or "Co_s," signifying "cobalt as surface CoO" (*26*). This Co phase appears to be responsible for a large part of the HDS activity (*2, 28*). Also in the pseudointercalation model the presence of such a sulfided Co species is presumed (*8, 9*).

Spectroscopic means, on the one hand, have not been able to discern the third oxidic phase from the β- or δ-phases. As shown above, measurement of chemical reactivity, on the other hand, appears to be promising in order to discriminate between the three Co phases (*26*). Therefore it is interesting to measure in detail the chemical reactivity of oxidic Co phases, e.g., the reducibility by means of Temperature-Programmed Reduction (TPR) (*29–31*).

It is the aim of the present study to elucidate the structure of CoO/Al_2O_3, prepared in various ways, and to illustrate the sensitivity of TPR applied to CoO/Al_2O_3. This system shows a large complexity, in contrast to the simplicity suggested by a two-phase model. In particular, the existence of at least four different Co phases will be shown.

EXPERIMENTAL

(*a*) *Materials.* Co_3O_4, $Co(NO_3)_2 \cdot 6H_2O$, and $Al(NO_3)_3 \cdot 9H_2O$ of pro analysi quality were used. The Al_2O_3 support was a high-purity γ-Al_2O_3 (Ketjen 000-1,5E (CK 300); specific surface area 195 m^2/g; pore volume 0.50 cm^3/g; particle size 100–150 μm). CoO was prepared from Co_3O_4, by heating at 1280 K in air for 22 h, followed by cooling to room temperature in N_2. $CoAl_2O_4$ was prepared from a coprecipitate of $Co(NO_3)_2 \cdot 6H_2O$ and $Al(NO_3)_3 \cdot 9H_2O$ (atomic ratio Co/Al: 0.5). This coprecipitate was calcined at 1220 K for 8 h, subsequently ground and calcined again at 1220 K for 20 h. A second Co–Al oxide was prepared from another coprecipitate of $Co(NO_3)_2 \cdot 6H_2O$ and $Al(NO_3)_3 \cdot 9H_2O$ (atomic ratio Co/Al: 2.0). Calcination at 925 K in an air flow for 2 h resulted in a mixed oxide, referred to as Co_2Al-oxide.

The 9.1 wt% CoO/Al_2O_3 catalysts were prepared by pore volume impregnation of γ-Al_2O_3 with a solution of $Co(NO_3)_2 \cdot 6H_2O$ in demineralized H_2O, followed by drying and calcining. Drying was performed at atmospheric pressure in air, by gradually increasing the temperature from 325 to 380 K over a period of 3 h, followed by an isothermal period of 16 h at 380 K. Dried samples of 0.5–1.0 g were calcined in a quartz tube (internal diameter 10 mm); they were heated to the final calcination temperature (575–1290 K) in a flow of purified N_2, at a heating rate of ca. 20 K/min, and were calcined at this temperature for 2 h in a flow of purified air. Purification of N_2 and air was necessary in order to prevent carbon deposition on the catalysts. Two series of

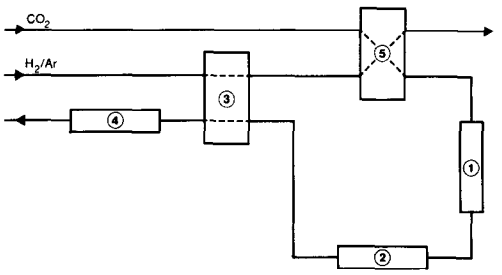

FIG. 1. Scheme of the TPR apparatus. (1) Reactor; (2) molecular sieves; (3) thermal conductivity detector; (4) flame ionization detector; (5) eight-way injection valve.

catalysts have been prepared. In Series 1 the calcination temperature was varied (575–1290 K), while the calcination flow rate was 70 μmol/s. In Series 2 the catalysts were calcined at 825 K, while the flow rate during calcining was varied (10–1000 μmol/s).

The materials used have been analyzed over a period of 1½ years. Therefore these samples contain large amounts of H_2O and can contain some organics.

(*b*) *X-Ray diffraction* (*XRD*). XRD has been carried out in a Philips diffractometer PW 1050/25 using Co$K\alpha$ radiation (wavelength 179.02 pm). A Fe filter was applied to remove Co$K\beta$ radiation. Crystallite sizes have been calculated using the Scherrer equation with correction for natural line broadening and assuming that the crystallite-shape factor K equals 1 (*32*).

(*c*) *Diffuse reflectance spectroscopy* (*DRS*). DRS measurements have been carried out in a Cary 14 spectrophotometer. Samples were ground and painted on $MgCO_3$ surfaces. DRS was measured against a $MgCO_3$ reference from 1800 to 300 nm.

(*d*) *Temperature-programmed reduction* (*TPR*). A schematic picture of the TPR apparatus is shown in Fig. 1. A high-purity mixture of 67% H_2/Ar (flow rate 12 μmol/s; pressure 1.0 bar) was passed, without further purification, over the oxidic samples in a quartz reactor tube (internal diameter 4–5 mm). The sample was held between two quartz wool plugs. The temperature of the sample was increased from room temperature up to 1240 K in a linear temperature program (10 K/min, if not stated otherwise). Subsequently the sample was kept at 1240 K for ca. 30 min. The amount of sample used in TPR analysis was varied in order to fix the amount of H_2 consumed on ca. 50–100 μmol (at 10 K/min). At other heating rates the amount of sample was changed in order to keep the H_2 conversion in the same range. H_2O, formed by reduction or dehydration, was trapped in 3A and 5A molecular sieve columns. Several other desorbing species, such as CO_2 and organics, were also trapped in these columns. After the gas mixture had passed through the molecular sieves, its composition was monitored continuously with a thermal conductivity detector (TCD) and a flame ionization detector (FID). The TCD detects all changes in the gas phase (caused by H_2, NO, NO_2, O_2, and CH_4 pressure changes). The FID is selective for CH_4, but also NO and NO_2 are detected (ca. 30 times less sensitive than CH_4). *Relative* sensitivities of TCD (for H_2 and CH_4) and FID (for CH_4) have been determined by means of reduction of CO_2 pulses in H_2/Ar at ca. 750 K over reduced Co catalysts. The CO_2 pulses (3.0 μmol) were introduced via a Carle eight-way injection valve. The Co catalysts used had been reduced at 1240 K for 30 min. Quantitative analysis showed complete conversion of CO_2 to CH_4; no CO was detected. Figure 2 shows the response of the TCD and FID to such a CO_2 pulse. Both H_2 consumption (4 H_2/CO_2) and CH_4 production (1 CH_4/CO_2) were detected by the TCD as a decrease of the thermal conductivity of the H_2/Ar mixture. It can be seen that CH_4 is retarded in the molecular sieves by 2.5 min. The *absolute* sensitivity of the TCD has been determined by TPR of high-purity V_2O_5, in which V_2O_5 is reduced to V_2O_3 (see Fig. 5f). The H_2 consumed in reduction of Co oxidic phases was calculated from the TCD signal after correction for CH_4 formed by reduction of organics,

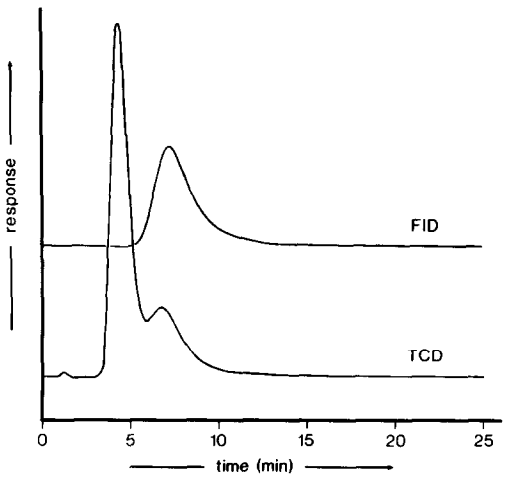

FIG. 2. Response of the thermal conductivity detector (TCD) and the flame ionization detector (FID) on injection of a pulse of CO_2 in H_2/Ar over a reduced 9.1% CoO/Al_2O_3 catalyst at 750 K. The catalyst was calcined at 625 K and reduced at 1240 K during 30 min in a normal TPR experiment.

which were adsorbed on quartz wool and on catalyst samples during storage. It is assumed that these organics consist of (polymerized) acetone (*33*). Acetone, used in large amounts in our laboratory, is extremely volatile, adsorbs strongly on CoO/Al_2O_3 samples, and can be reduced completely to CH_4 at 675 K over reduced CoO/Al_2O_3. Reduction of acetone requires consumption of 4 H_2 and results in production of 3 CH_4, so $\frac{4}{3}$ H_2 is consumed per CH_4 produced. The TPR peak area, calculated from the TCD signal, is corrected assuming that all CH_4 is generated by acetone reduction. The overall error in the corrected H_2 consumption values was ca. 10%.

RESULTS

(*a*) *X-Ray Diffraction*

Co_3O_4 and $CoAl_2O_4$ are XRD-pure and show the expected spinel patterns with a calculated cell constant of 806.9 and 809.0 pm, respectively. These values agree well with the literature values of 808.5 pm (ASTM 9-418) and 810.5 pm (ASTM 10-458), respectively. The XRD pattern of CoO shows the presence of traces of Co_3O_4, indicating some reoxidation of CoO at room temperature after the preparation from Co_3O_4 at high temperature. Co_2Al-oxide shows only spinel lines with a cell constant of 807.9 pm.

Figure 3 shows the XRD patterns of 9.1% CoO/Al_2O_3 catalysts, calcined at various temperatures (Series 1). The dried catalyst shows only the broad lines of the γ-Al_2O_3 support. The catalysts calcined at 575–1175 K show also spinel lines of low intensity. For calcination temperatures between 575 and 900 K the intensity of these lines does not change and a cell constant of 807 pm is calculated, using the (311) reflection. For calcination temperatures above 900 K the intensity of the lines increases and simultaneously the lines shift until for the 1175 K calcined sample a cell constant of 796.5 pm (calculated on the basis of the five strongest

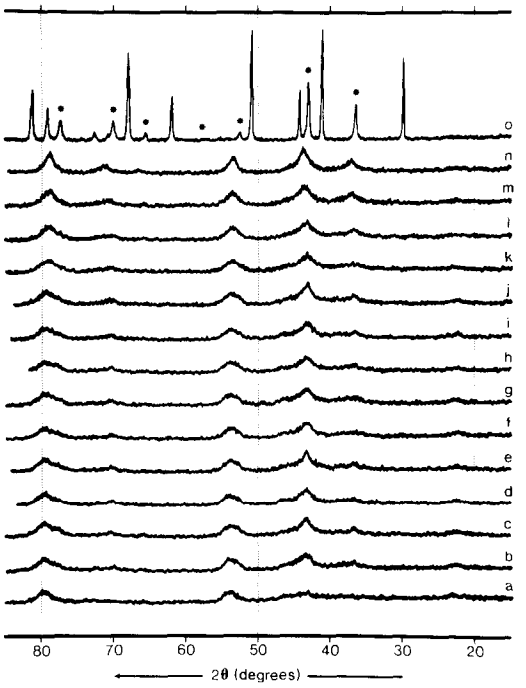

FIG. 3. XRD patterns of 9.1% CoO/Al_2O_3 catalysts calcined at various temperatures (Series 1). Calcination temperature (K): 380 (a), 575 (b), 625 (c), 675 (d), 725 (e), 775 (f), 825 (g), 875 (h), 900 (i), 925 (j), 975 (k), 1025 (l), 1075 (m), 1175 (n), 1290 (o). The asterisks give the XRD line positions of $CoAl_2O_4$ (ASTM 10-458).

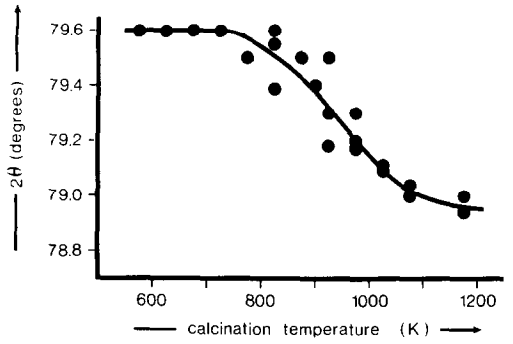

FIG. 4. The 2θ-value of the (440) reflection as a function of calcination temperature of 9.1% CoO/Al_2O_3 catalysts (Series 1).

reflections) is reached. The crystallite size is 11 ± 2 nm, independent of calcination temperature in the range 575–1175 K. The sample calcined at 1290 K shows very sharp lines, which originate from α-Al_2O_3 and $CoAl_2O_4$.

Figure 4 shows the 2θ-value of the (440) reflection as a function of calcination temperature. The 2θ-value of catalysts calcined below 800 K is almost identical to the value of the pure support (79.7°). Calcination temperatures above 800 K result in a decrease of the 2θ-value, until at 1175 K a value of 79.0° is reached. This decrease of 2θ corresponds with an increase of the cell constant from 791 to 796 pm. In fact, diffraction lines of Al_2O_3 and Co oxides of spinel type blend together into one spinel pattern with a cell constant of 796 pm. No δ-Al_2O_3 (2θ-value of (440) reflection at 79.9°) is detected on the catalysts, independent of calcination temperature, whereas in separate experiments it was shown that δ-Al_2O_3 is formed from unloaded Al_2O_3 by calcination at ca. 1175 K.

Variation of the calcination flow rate (Series 2) shows a marked influence on the XRD pattern. A drastic increase of flow rate (from 70 to 1000 μmol/s) results in disappearance of the catalyst spinel lines.

(b) Colors

For the catalysts some color changes can be easily observed with the eye. Dried catalysts are pink. Catalysts calcined between 575 and 975 K are colored dark green to black. Calcination between 1025 and 1290 K results in blue samples. However, also some more subtle color changes have been observed, which have been checked with DRS. The catalysts calcined at 1025–1175 K are deep blue (strong triplet around 600 nm), whereas $CoAl_2O_4$ and the catalyst calcined at 1290 K are more brightly blue-colored (absorption around 350 nm, besides the strong triplet around 600 nm). The increase of the calcination flow rate leads to a color change from dark green to lighter green, which correlates with the disappearance of absorption around 800 nm in DRS.

(c) Temperature-Programmed Reduction

The Figs. 5–9 show the TPR results. Each TPR pattern consists of a TCD pattern (upper line) and a FID pattern (lower line), as a function of reduction temperature. CH_4 production takes place at somewhat lower temperatures than is shown in the figures, because of CH_4 retardation in the molecular sieves (e.g., a 25 K shift at a heating rate of 10 K/min). Table 1 gives the quantitative TPR results.

Figure 5 shows the TPR patterns of bulk compounds. Some CH_4 formation occurs for all Co compounds. A prerequisite for CH_4 formation appears to be the formation of metallic Co. CoO and Co_3O_4 give one relatively sharp reduction peak at 610 and 590 K, respectively. The Co_3O_4 peak is broader than the CoO peak, indicating that in fact two reduction steps ($Co^{3+} \rightarrow Co^{2+} \rightarrow Co^0$) take place. $CoAl_2O_4$ reduces at a quite high temperature (1160 K), except for a small peak at 770 K due to reduction of an impurity. In the case of CoO, Co_3O_4, and $CoAl_2O_4$ the amount of H_2 consumed in TPR agrees with complete reduction to metallic Co. Co_2Al-oxide shows three reduction peaks at 610, 725, and 1050 K (35, 60, and 5% of the H_2 consumption, respectively). The support material γ-Al_2O_3 has a peak at 1120 K, which is probably due to

TABLE 1

Quantitative TPR Results

Materials	Heating rate (K/min)	H_2 consumption[a] (mol H_2/mol M)	CH_4 production[a] (mol CH_4/mol M)	NO_x production[a] (mol NO_x/mol M)
Bulk compounds				
CoO	10	1.16	0.04	—
Co_3O_4	10	1.39	0.05	—
Co_2Al-oxide	10	1.39	0.07	—
$CoAl_2O_4$	10	1.06	<0.01	—
γ-Al_2O_3	10	0.0035	<0.01	—
V_2O_5	10	1.00	<0.01	—
		9.1% CoO/Al_2O_3 catalysts		
Series 1: calcination temperature (K)				
380	10	1.01[b]	0.11	2.0[c]
575	10	1.22[b]	0.06	0.29
625	10	1.15[b]	0.09	0.05
675	10	1.17	0.11	—
725	10	0.99	0.13	—
775	10	1.11	0.07	—
825	10	1.18	0.07	—
875	10	1.10	0.11	—
900	10	1.05	0.09	—
925	10	1.34	0.08	—
975	10	1.02	0.07	—
1025	10	1.11	<0.01	—
1075	10	0.97	<0.01	—
1175	10	0.88	<0.01	—
1290	10	0.98	<0.01	—
Series 2: calcination flow rate (μmol/s)				
10	10	1.45	0.14	—
70	2	1.27	0.08	—
70	10	1.21	0.09	—
70	35	1.16	0.17	—
1000	10	1.07	0.07	—

[a] M is Co, except for the samples γ-Al_2O_3 and V_2O_5; H_2 consumption is corrected for CH_4 formation and, in the case of CoO/Al_2O_3 catalysts, for H_2 consumption of the support.

[b] H_2 consumption is only calculated for the temperature region above the nitrate decomposition peak.

[c] NO_x production is calibrated assuming that the dried catalyst has not lost any N as NO_x or HNO_3.

reduction of traces of impurities, such as iron, sulfite, and sulfate.

Figure 6 shows the TPR patterns of a catalyst (Series 2), measured at different heating rates. The TPR peaks shift to higher temperatures with increasing heating rate, as expected (*34, 35*). More CH_4 is produced at the highest heating rate. But, corrected for CH_4 production, the TPR *pattern* is essentially independent of the heating rate.

In Fig. 7 the calcination temperature is varied (Series 1). Several overlapping peaks can be discerned in the range 500–1240 K. Figure 8 summarizes the position of the main TPR peak maxima as a function of calcination temperature. For very low calcination temperatures (380–625 K) a peak occurs at ca. 500 K for both TCD and FID. This can be attributed to H_2-assisted decomposition of Co nitrate species (evolu-

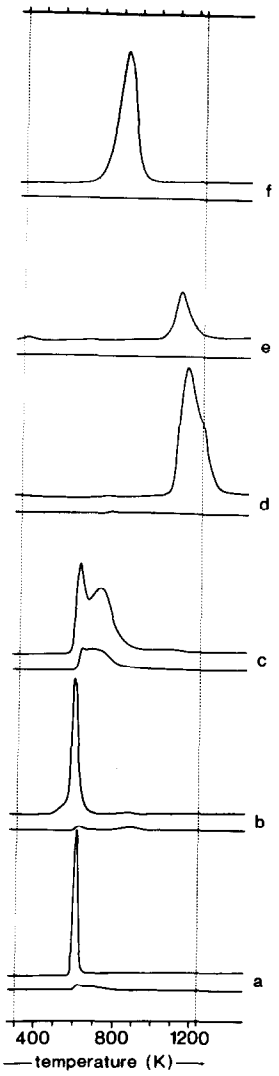

FIG. 5. TPR patterns of reference materials. (a) CoO; (b) Co_3O_4; (c) Co_2Al-oxide; (d) $CoAl_2O_4$; (e) γ-Al_2O_3; (f) V_2O_5. The upper and lower part of each pattern represent the TCD and FID signal, respectively.

tion of NO and NO_2). Apparently nitrate can only be removed completely by calcination at ca. 650 K. Furthermore, large amounts of CH_4 (ca. 0.1 CH_4/Co) are found around 720 K for calcination temperatures between 380 and 975 K. Moreover, five peaks are assigned to reduction of Co ions:

—At 515 K, for calcination temperatures between 675 and 875 K.

—At 560–630 K. This peak is relatively sharp and shifts 70 K to higher temperature when the calcination temperature is increased from 575 to 875 K. For calcination temperatures above 900 K this peak is absent.

—At 740 K, for calcination temperatures up to 975 K. Note that this peak has to be attributed mainly to CH_4 formation for calcination temperatures up to 775 K.

—At 875 K, for calcination temperatures up to 900 K.

—At 1110–1230 K. The peak maximum occurs around 1110 K for samples calcined below 900 K and shifts to ca. 1230 K for the sample calcined at 1175 K. Calcination at 1290 K, however, leads to a decrease of the reduction temperature to 1150 K. The intensity is constant for calcination temperatures below 775 K, but increases continuously for calcination temperatures above 775 K, until all reduction takes place in this region, for samples calcined at 1025 K or higher.

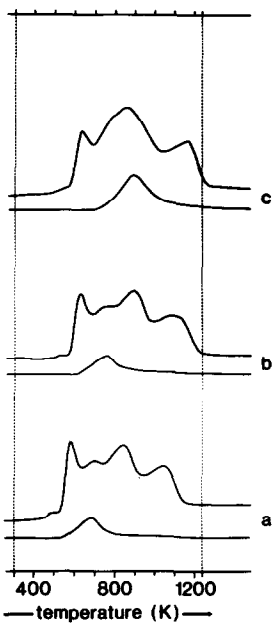

FIG. 6. TPR patterns of a 9.1% CoO/Al_2O_3 catalyst (Series 2) at various heating rates. (a) 2 K/min; (b) 10 K/min; (c) 35 K/min. The catalyst was calcined at 825 K in a flow of 70 μmol/s. The upper and lower part of each pattern represent the TCD and FID signal, respectively.

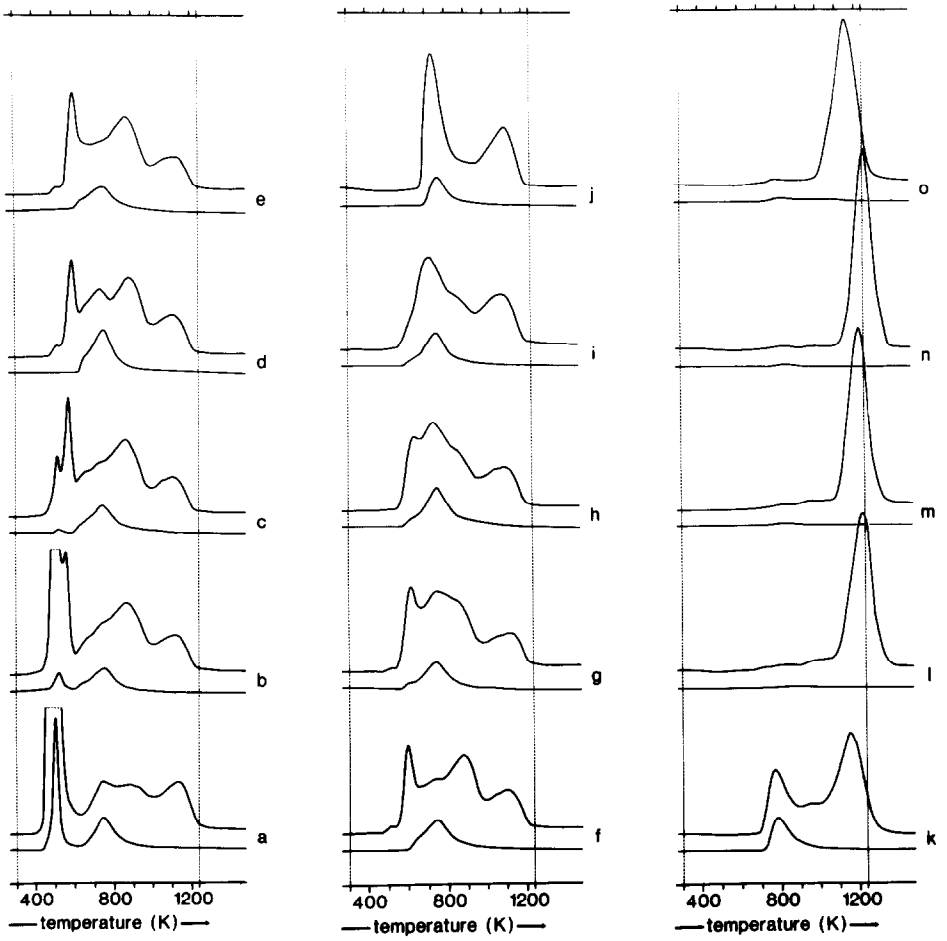

FIG. 7. TPR patterns of 9.1% CoO/Al_2O_3 catalysts calcined at various temperatures (Series 1). Calcination temperature (K): 380 (a), 575 (b), 625 (c), 675 (d), 725 (e), 775 (f), 825 (g), 875 (h), 900 (i), 925 (j), 975 (k), 1025 (l), 1075 (m), 1175 (n), 1290 (o). The upper and lower part of each pattern represent the TCD and FID signal, respectively.

From the H_2 consumption values (see Table 1) it is clear that for calcination temperatures below 1025 K, besides Co^{2+} ions, also Co^{3+} ions are present, whereas above 1025 K only Co^{2+} ions exist.

Figure 9 shows the TPR patterns of catalysts for which the calcination flow rate was varied (Series 2). The reduction peaks are found at the same temperatures as in Fig. 7. With increasing flow rate, the contribution of peaks at low temperature declines. The overall H_2 consumption decreases sharply as a function of flow rate, approximately from 1.5 to 1.0 H_2/Co. In separate experiments it was shown that an increase of catalyst weight during calcination has the same influence on the TPR pattern as a decrease of flow rate.

DISCUSSION

(a) *Interpretation of the TPR Patterns*

The results show the complexity of CoO/Al_2O_3. Therefore it is not surprising that previous studies, which contain only a limited number of TPR measurements (*22, 36*), have not led to new insight in the structure of CoO/Al_2O_3. In this discussion a detailed interpretation will be presented, which is tentative in part, but which is consistent

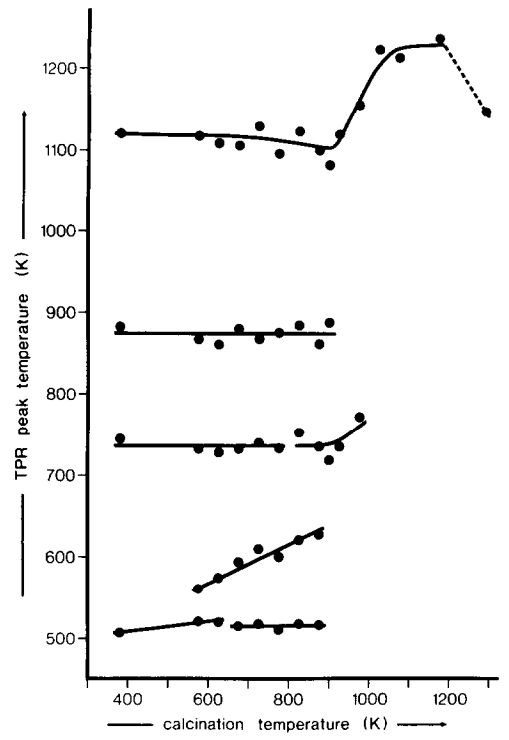

FIG. 8. The position of the main TPR peak maxima (TCD detection) as a function of calcination temperature of 9.1% CoO/Al_2O_3 catalysts (Series 1).

with the literature (see the Introduction). There are parallels between this work and recently published work on coprecipitated NiO/Al_2O_3 catalysts (*37*), which contains also XRD and TPR results. Especially conclusions on the presence of spinel-type mixed Ni/Co–Al-oxides of various composition and on the role of solid-state diffusion in their interconversions are common features.

It is surprising that the reduction of Co ions takes place over such a large range of temperatures. $CoAl_2O_3$ reduces at much higher temperatures than CoO and Co_3O_4, obviously due to the presence of Al^{3+} ions. Therefore, it is suggested here that, for crystalline as well as for surface species, the number of Al^{3+} ions in the surrounding of the Co ion determines the TPR reduction temperature mainly, while Co valency, coordination, and nucleation are less important. This can be supported by consideration of the partly covalent character of transition metal ions in spinels (*38*). Probably Al^{3+} ions polarize the more or less covalent Co–O bonds. This will increase the effective charge of the Co ions (*39*) and, as a consequence, the lattice energy, resulting in an increase of reduction temperature. This so-called polarization concept has been used successfully to explain temperature-programmed reduction and sulfiding patterns of MoO_3/Al_2O_3 catalysts (*40*).

For the interpretation of the TPR patterns it is assumed that reduction of Co^{3+} and Co^{2+} to Co metal during TPR generally takes place in one peak, leading to assignment of the various reduction peaks to different Co phases. Some partial reduction of Co^{3+} to Co^{2+}, however, might take place below 550 K in the case of bulk Co_3O_4 (slightly broadened TPR peak) and some catalysts (small peak at 515 K).

Figure 10 summarizes the position of the main TPR peaks schematically. Four main

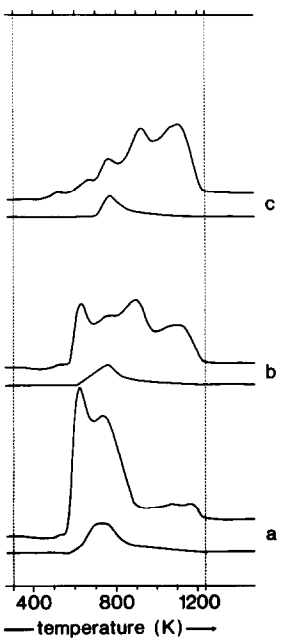

FIG. 9. TPR patterns of 9.1% CoO/Al_2O_3 catalysts calcined at 825 K at various flow rates (Series 2). (a) 10 μmol/s; (b) 70 μmol/s; (c) 1000 μmol/s. The upper and lower part of each pattern represent the TCD and FID signal, respectively.

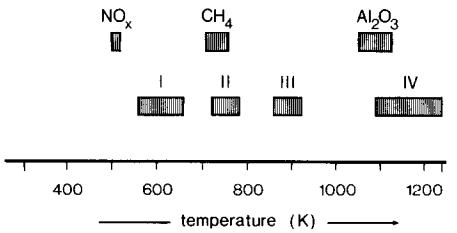

FIG. 10. Scheme of the position of the main TPR peak maxima.

reduction regions (I, II, III, and IV) are observed, which correspond to four different phases, referred to as phases I, II, III, and IV, respectively.

It has to be stressed that TPR analysis is a destructive measurement. Especially solid-state diffusion of Co^{2+} ions might interfere with reduction. Since in the present study solid-state diffusion is observed in the case of calcination above 800 K for 2 h, the reduction of the phases I and II, of phase III, and of phase IV are expected to be disturbed not at all, slightly and strongly, respectively. In agreement with this, the invariability of the TPR peak areas of regions III and IV as a function of heating rate, for a catalyst calcined at a temperature (825 K) where the influence of solid-state diffusion is marginal (see Fig. 6), suggests that reduction in region III is not significantly affected by solid-state diffusion. Since, therefore, only phase IV will be affected, it is reasonable to assume that TPR gives an essentially correct distribution of Co ions over the phases.

Figure 11 shows a scheme of the presence of the various Co phases, as a function of calcination temperature. The various reduction regions are assigned to Co phases as follows.

Region I. Reduction of CoO and Co_3O_4 crystallites takes place in this region. Reduction of catalysts in region I is attributed to reduction of Co_3O_4 crystallites, since the presence of CoO crystallites is unlikely on the basis of XRD data. Moreover, CoO is not a stable phase in the presence of O_2 at temperatures between 600 and 1000 K (*41*). The sharpness of the region I peak points to the presence of well-defined, crystalline material. Generally Co_3O_4 is described in the literature as the main oxidic phase at high loadings. Assuming that Co_3O_4 exclusively reduces in region I, the present study shows that no 9.1% CoO/Al_2O_3 sample contains more than 25% of the Co as Co_3O_4.

Region IV. Reduction in this region is observed for $CoAl_2O_4$ crystallites as well as for all catalyst samples. XRD data show that the catalyst calcined at 1290 K contains stoichiometric $CoAl_2O_4$ (phase IVD), besides α-Al_2O_3. The catalysts calcined at 1025–1175 K also contain phase IV exclusively, but they differ from $CoAl_2O_4$ on the basis of XRD, color (DRS), and TPR data. It is concluded that these catalysts contain

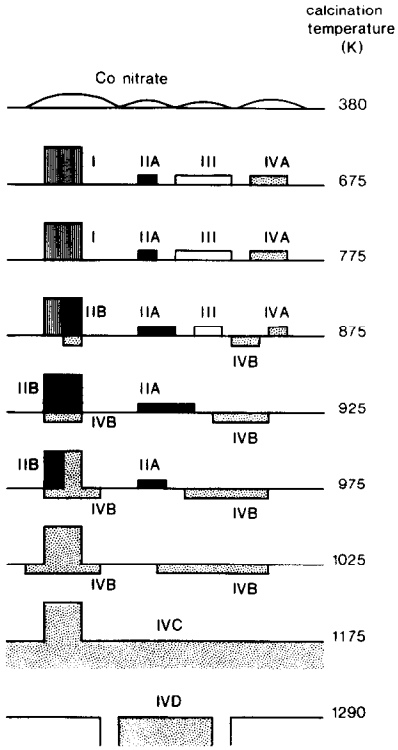

FIG. 11. Scheme of the various Co phases present on 9.1% CoO/Al_2O_3 catalysts as a function of calcination temperature (Series 1). Crystalline and surface species are presented on the left and right, respectively. The assignment of the phases is summarized under Conclusions.

a Co^{2+}–Al^{3+} spinel structure (phase IVB) in which Co^{2+} is present in a diluted form in comparison with $CoAl_2O_4$. Especially calcination at 1175 K leads to small particles of a well-defined solid solution (phase IVC) of spinel type with the formula $Co_xAl_{(8/3-2/3x)}O_4$ ($0 < x < 1$; $x = 0.18$ in this study), which has its own XRD, DRS, and TPR characteristics. The amount of phase IV increases with increasing calcination temperature in the range 825–1025 K, showing the diffusion of Co^{2+} ions into the Al_2O_3 lattice. But also for lower calcination temperatures phase IV is present, in a constant amount, which cannot be formed by solid-state diffusion. Therefore, in the latter case phase IV is assumed to consist of surface Co^{2+} ions (phase IVA) with a high number of O–Al ligands, which makes them behave chemically like $CoAl_2O_4$. The increase of reduction temperature of phase IV as a function of calcination temperature (see Fig. 8) probably indicates that the lattice stabilization of Co^{2+} ions increases with advancing solid-state diffusion. It cannot be excluded, however, that this reduction temperature increase is caused partly by a decrease of catalytic H_2 dissociation over Co metal sites, due to a decrease of the Co metal concentration present at the beginning of the region IV TPR peak.

Region III. Reduction in this region is only found for catalyst samples calcined below ca. 950 K. Variation of the calcination flow rate (see Fig. 9) showed that especially at high flow rate phase III dominates, besides phase IV, and that the H_2 consumption approaches the value of 1 H_2/Co, suggesting that phase III is a Co^{2+} phase. The fact that the catalyst sample calcined at high flow rate did not show any XRD spinel lines and the absence of phase III in bulk compounds indicate that phase III is a surface phase of Co^{2+} ions.

Region II, phase IIB. Reduction in region II has been found for bulk Co_2Al-oxide and for catalysts calcined below ca. 1000 K. There is evidence that reduction in this region is due to reduction of Co^{3+} ions:

—From the TPR peak area of bulk Co_2Al-oxide a H_2 consumption of phase II of 1.45 H_2/Co can be calculated, after correction for the H_2 consumption of the phases I and IV.

—Variation of the calcination flow rate (see Fig. 9) showed that at low flow rate, where phase II is dominating besides phase I, and H_2 consumption approaches the value of 1.5 H_2/Co.

Moreover, there is evidence that phase II can have a crystalline spinel structure:

—XRD of bulk Co_2Al-oxide shows only spinel lines.

—XRD of catalysts calcined at 900–975 K, which contain no phase I, show also this spinel pattern.

—The sharpness of the phase II reduction peak for catalysts calcined at 900–975 K suggests the presence of well-defined crystalline material.

Two possibilities arise for the assignment of a crystalline phase IIB. It consists either of Co_3O_4 crystallites of a morphology different from phase I or of a novel mixed Co^{3+}–Al^{3+}-oxide. In the former case the different reducibility of the phases I and II is supposed to be related to different reduction mechanisms due to differences in particle size or concentration of surface defects. Although changes in Co_3O_4 morphology might explain, e.g., the 70 K upward shift of the region I peak with increasing calcination temperature (see Discussion, part below), assignment of region II to Co_3O_4 crystallites is not likely for the following reasons:

—Essentially, phase II reduction is always found at the same temperature, independent of calcination temperature, particle size, and concentration of Co metal sites, needed for catalytic H_2 dissociation, present at the beginning of the region II TPR peak (*35*).

—The difference in reducibility of phases I and II is quite large (110–180 K).

On the other hand, the assignment of phase IIB to a mixed Co–Al-oxide can be supported as follows:

—Interaction compounds may be ex-

pected using the coprecipitation method (*37*).

—The difference in reducibility of phases I and II can easily be explained by the presence of Al^{3+} ions in phase II, via the polarization concept.

—The simultaneous disappearance of Co_3O_4 crystallites of phase I and the growth of the phase II TPR peak occurs in the calcination temperature range 875–925 K, i.e., at temperatures where solid-state diffusion of Co^{2+} ions takes place at a reasonable rate. This suggests that Co^{2+} ions from Co_3O_4 can be exchanged with Al^{3+} ions of the support, resulting in formation of a mixed Co^{3+}–Al^{3+}oxidic crystalline phase.

The following considerations might specify the identity of this spinel-type mixed oxide:

—Co^{2+}, Co^{3+}, and Al^{3+} ions occur abundantly in spinel-type structures. Co_3O_4 and $CoAl_2O_4$ are normal spinel structures, with Co^{2+} on tetrahedral and Co^{3+} and Al^{3+} on octahedral positions. Also γ-Al_2O_3 is generally considered to be an (imperfect) spinel (*42*) where the Al^{3+} ions fill $\frac{2}{3}$ of the tetrahedral in addition to the octahedral spinel cation positions (*43*).

—Calculations based on ligand field theory show a large relative octahedral site preference energy of Co^{3+} with respect to Al^{3+} (43 kJ/mol; see the Appendix). Therefore, in the mixed oxide Co^{3+} is expected to win the competition for the octahedral spinel positions and Al^{3+} might be present only on tetrahedral sites.

—The conversion of Co_3O_4 into the mixed oxide on catalysts at 875–925 K is suggested in the above to occur via solid-state diffusion. Co^{2+}–Al^{3+} exchange is most reasonable from a kinetic point of view when it is limited to tetrahedral sites, since in this way the position of the Co^{3+} ions is not affected.

The above-mentioned arguments lead to a tentative overall formula of the mixed oxide of $Al^{3+}_{2/3}(Co^{3+}_2)O^{2-}_4$ or Co_3AlO_6, where Co^{3+} ions occupy all the octahedral spinel sites, as in Co_3O_4, and Al^{3+} ions occupy the tetrahedral sites, as they do partly in γ-Al_2O_3.

Region II, phase IIA. It is obvious that in a catalyst system which is quite well-dispersed and can contain such a large fraction of (sub)surface Co^{2+} ions, also Co^{3+} surface ions can occur. There is some evidence that in region II, being typical for Co^{3+} ions, also surface Co^{3+} ions (phase IIA) can reduce:

—Region II is present for catalysts calcined below 825 K. At these low temperatures solid-state diffusion is slow or absent, which excludes the formation of crystalline Co_3AlO_6 and, therefore, points to the presence of a dispersed Co^{3+} phase.

—The reduction peak in region II is broader after calcination at 875 K than after calcination at 925 K, suggesting more interaction of Co ions with the heterogeneous support for the 875 K calcined sample.

—An increase of calcination temperature from 775 to 925 K leads to conversion of phase III species into phase II and phase IV species. As phase III consists of surface ions, it is likely that from phase III surface phase II species are formed.

Co coordination. In phases IVB, IVC, and IVD the Co^{2+} ions are forced to occupy bulk tetrahedral lattice sites, as a consequence of the unfavorable relative octahedral site preference energy of Co^{2+} ions with respect to Al^{3+} ions (−54 kJ/mol; see Appendix). In the case of the phases III and IVA (surface Co^{2+} ions) no competition is present between Co^{2+} and Al^{3+} ions, since excess tetrahedral and octahedral sites are available for the Co^{2+} ions. Therefore in the latter case the absolute octahedral site preference energy of Co^{2+} ions has to be considered (8 kJ/mol; see Appendix). This preference for octahedral sites is in agreement with recent literature (*27*). The favored coordination of Co^{3+} ions (phase II) is undoubtedly octahedral.

In the above-mentioned polarization concept the reducibility of the various Co phases is related to the number of Al^{3+} ions in the Co surroundings:

—Phase I (Co_3O_4 or CoO) containing no Al^{3+} ions reduces at the lowest tempera-

ture, whereas phases IVB, IVC, and IVD containing 12 Al^{3+} ions in the first shell reduce at the highest temperature.

—The difference in reducibility between the phases IVC and IVD (reduction temperatures of 1230 and 1150 K, respectively) can be explained considering the number of Al^{3+} ions beyond the first shell; in the more diluted spinel of phase IVC, Co^{2+} is surrounded by many more Al^{3+} ions in the long range, resulting in slightly more polarization and, therefore, a decreased reducibility.

—The Co^{2+} surface ions of phase IVA, having a reducibility similar to that of the phases IVB, IVC, and IVD, are proposed to have also a similar number of Al^{3+} neighbors allowing minimum surface properties, i.e., ca. 10 Al^{3+} ions in the first shell.

—The number of Al^{3+} in the Co^{3+} surroundings in the proposed Co_3AlO_6 crystallites is low (4 Al^{3+} ions in the first shell). Such a value is reasonable for surface Co^{3+} ions and explains the fact that the reducibility of surface Co^{3+} ions is similar to that of Co_3AlO_6 crystallites.

—Because of its intermediate reducibility, the number of Al^{3+} ions around phase III Co^{2+} ions is expected to lie between those of the phases II and IV (ca. 4 and 10–12 Al^{3+} ions, respectively) and therefore is estimated to be 6–8.

(*b*) *Dynamics of the Preparation of Oxidic Co Catalysts*

Influence of the calcination flow rate. The calcination flow rate influences the catalyst structure strongly (see Fig. 9). This is explained tentatively by the interference of NO_2, a much stronger oxidant than O_2 and found in the present study as a primary product of nitrate decomposition during calcination. The NO_2 concentration will depend on the calcination flow rate, on calcination sample weight, on reactor geometry, and on heating rate. So, keeping all other parameters constant, the flow rate during calcination determines the NO_2 concentration in the catalyst particle. Apparently NO_2 is able to oxidize Co^{2+} to Co^{3+} easily below 825 K. In this perspective it is understood why the Co^{2+} phases III and IV are formed at high flow rates, whereas, at low flow rates, the Co^{3+} containing phases I and II are formed.

Even the dispersion is affected by the calcination flow rate. From XRD data it is concluded that Co nitrate species on the dried catalyst are well dispersed, while at least part of the Co is assumed to be present as poorly crystalline, very small droplets of Co nitrate. By calcination at 575 K or higher these droplets decompose, resulting in the production of mobile Co^{2+} ions. In the absence of NO_2, these ions will distribute themselves over the surface and will constitute the well-dispersed phases III and IVA. Oxidation of Co^{2+} to Co^{3+} by NO_2, on the other hand, prevents this dispersion; Co_3O_4 crystallites are formed. XRD data show that these crystallites are larger than the original Co nitrate droplets, illustrating again the mobility of Co^{2+} ions.

Influence of the calcination temperature. The drastic influence of calcination temperature (see Fig. 11) can be explained by a combination of oxidation and reduction phenomena and solid-state diffusion of Co^{2+} ions. Crystallite morphology plays a minor role.

(*i*) *Oxidation and reduction phenomena.* Oxidation of Co^{2+} to Co^{3+} has been shown to be an easy reaction with NO_2 as oxidant. However, also oxidation of Co^{2+} by O_2 is observed in the calcination temperature range 775–925 K (conversion of phase III to phase II). Above a calcination temperature of ca. 950 K reduction of Co^{3+} to Co^{2+} takes place, which is observed as the conversion of phase II (main phase at 925 K) to phase IV (only phase at 1025 K). This reduction is also found for the bulk-phase Co_3O_4; even in air it reduces to CoO around 1000 K (*41*).

(*ii*) *Solid-state diffusion of Co^{2+}* ions. Solid-state diffusion of Co^{2+} ions takes place at temperatures of ca. 800 K and higher. This follows from both XRD and TPR measurements. XRD shows the ex-

pansion of the oxidic Al_2O_3 lattice caused by the entrance of Co^{2+} ions into the bulk. TPR shows that the amount of phase IV increases in the same temperature range. Solid-state diffusion of Co^{2+} ions (above ca. 800 K) and reduction of Co^{3+} to Co^{2+} (above ca. 950 K) lead to complete conversion of the phases I, II, and III into phase IV around 1000 K. However, this conversion is not always a one-step reaction. Co_3O_4 crystallites (phase I) are supposed to be transformed first, around 875 K, into phase IIB plus phase IVB. Phase III is converted to phase IV by diffusion, but can also be oxidized to phase IIA.

(*iii*) *Crystallite morphology*. The region I peak of Co_3O_4 crystallites shifts to higher temperatures when the calcination temperature is increased (see Fig. 8). This shift cannot be explained by a crystallite size effect, because XRD calculations have shown that the crystallite size is constant. Probably higher temperatures lead to a loss of imperfections in the Co_3O_4 surface; in that case fewer reduction nuclei will be formed, shown as a slight upward shift of the reduction temperature.

(*c*) *Implications for $CoO–MoO_3/Al_2O_3$ HDS Catalysts*

In the following will be discussed the way in which the structural information on CoO/Al_2O_3 obtained in this study might be related to HDS activity of $CoO–MoO_3/Al_2O_3$ catalysts.

Loss of Co for HDS activity. Solid-state diffusion of Co^{2+} ions takes place already at ca. 800 K. This process is supposed to lead to loss of Co for the HDS reactions. Therefore a calcination temperature below 800 K is expected to give the highest HDS activity.

Stabilization of HDS-active Co–Mo phases. Al^{3+} ions might influence the structure of HDS-active sites. The main function of Al^{3+} ions in the surroundings of HDS-active sulfided Co–Mo phases is assumed to be the stabilization of these phases. Al^{3+} ions can polarize covalent Co–S and Mo–S bonds, as has already been described for Mo–S (*40*) and for Co–O bonds (in this article). This polarization will lead to stronger bonds and therefore will decrease dispersion loss of the sulfide phase under the corrosive HDS conditions. Because Co^{2+} diffusion into Al_2O_3 always goes together with Al^{3+} diffusion to the surface (above ca. 800 K), it is suggested that for $CoO–MoO_3/Al_2O_3$ catalysts calcined above 800 K some Al^{3+} ions can be present within the Co–Mo phases. In fact some active species might be described most accurately as mixed Co–Mo–Al-oxysulfides.

Sulfiding of oxidic Co phases. The oxidic Co phase which is the precursor of the HDS-active sulfided Co phase, is supposed to be "nonreducible" but sulfidable (see the Introduction). Only the Co phases III and IV can be considered to be nonreducible in normal isothermal reduction studies at typical temperatures of 675–775 K (*17, 18, 20, 24, 25*). As bulk $CoAl_2O_4$ (phase IVD) is reported to be "nonsulfidable" (*26*), it is concluded that also the bulk phases resembling $CoAl_2O_4$ (phases IVB and IVC) will be nonsulfidable. Only nonreducible surface Co^{2+} ions (phases III and IVA) might be sulfidable and therefore be the precursor of the HDS-active sulfide phase. It appears contradictory that phases which reduce with difficulty can be sulfided at normal temperatures. However, for surface Mo^{6+} ions on MoO_3/Al_2O_3 catalysts it has also been found that sulfiding is a much easier reaction than reduction (*40*). This difference is explained by the completely different mechanism of sulfiding, in which O–S exchange predominates and reduction with H_2 is only a secondary reaction.

CONCLUSIONS

1. In TPR measurements (10 K/min) of the CoO/Al_2O_3 system four different reduction regions have been observed, around 600, 750, 900, and 1150 K. These reduction regions have been assigned to four different Co phases (I, II, III, and IV, respectively), subdivided into eight subphases, as follows:

I, Co_3O_4 crystallites; IIA, surface Co^{3+} ions; IIB, mixed Co^{3+}–Al^{3+}-oxidic crystallites, probably of Co_3AlO_6 stoichiometry; III, surface Co^{2+} ions; IVA, surface Co^{2+} ions as in III, but with more Al^{3+} neighbors; IVB, subsurface Co^{2+} ions in a diluted, not well-defined Co^{2+}–Al^{3+} spinel; IVC, subsurface Co^{2+} ions as in IVB, but in a well-defined spinel of composition $Co_x Al_{(8/3-2/3x)}O_4$ ($0 < x < 1$); IVD, $CoAl_2O_4$ crystallites.

2. Besides reduction of Co ions also H_2-assisted decomposition of nitrate species (NO_x production) and Co-metal-catalyzed reduction of organic impurities such as (polymerized) acetone (CH_4 production) take place.

3. A novel compound of stoichiometry Co_3AlO_6 is proposed, having a spinel structure in which Co^{3+} and Al^{3+} ions fill the octahedral and tetrahedral sites, respectively. It is supposedly formed from Co_3O_4 crystallites by diffusion of Co^{2+} ions into and Al^{3+} ions out of the Al_2O_3 support, above ca. 800 K. It decomposes in air with reduction of Co^{3+} to Co^{2+} above ca. 950 K.

4. The valency of Co (2+ or 3+) depends on the concentration of NO_2 formed during calcination from the starting nitrates (oxidation) and on the calcination temperature (oxidation at 775–925 K; reduction above 950 K). The Co valency affects the dispersion; Co^{2+} ions distribute themselves, whereas in the presence of Co^{3+} ions sintering to Co_3O_4 crystallites takes place.

5. The rate of solid-state diffusion depends strongly on the calcination temperature and on the Co valency. Co^{2+} ions diffuse into the Al_2O_3 support both from well-dispersed Co^{2+} surface species and from Co_3O_4 crystallites (above ca. 800 K). Simultaneously Al^{3+} ions are forced to diffuse to the surface. These processes probably lead to loss of Co for HDS activity and to the potential presence of Al^{3+} ions within the HDS-active phases.

6. The concept of polarization of Co–O bonds by Al^{3+} ions can explain the TPR results on CoO/Al_2O_3. The same concept predicts increased stability of HDS-active sulfided Co–Mo phases by Al^{3+} ions, leading to a decrease of dispersion loss of these phases under the corrosive HDS reaction conditions.

APPENDIX

Calculation of Octahedral Site Preference Energies

(a) The octahedral site preference energy of Al^{3+}. In the literature the preference of transition metal cations for octahedral with respect to tetrahedral positions is presented in the form of octahedral site preference energies (*38, 44, 45*). For high-spin configurations the number of paired spins is the same for octahedral and tetrahedral surroundings. Therefore, ignoring the exchange energy, the octahedral site preference energy can be calculated from the value of the field splitting parameter *Dq* only (*38, 44*). In this way for Co^{2+} ions a preference energy of 8 kJ/mol is calculated (*38, 44*). For Al^{3+} ions no value can be obtained spectroscopically, since Al is not a transition metal. However, a relative octahedral site preference energy has been found for Al^{3+} with respect to Co^{2+} of 54 kJ/mol (*45*). From the two above-mentioned values an octahedral site preference energy value for Al^{3+} is calculated to be 62 kJ/mol.

(b) The Octahedral Site Preference Energy of Co^{3+}

Co^{3+} has special features within the range of transition metal ions, since it occurs in octahedral sites of spinels in the low-spin configuration (*38*). The *Dq* value of Co^{3+} is high enough to overcome the loss of stabilization caused by spin pairing. From a combination of literature values the octahedral site preference energy of Co^{3+} can be calculated by means of ligand field theory, as follows.

From *Dq* and the exchange energy parameter *K* (*46*) the following energies can be derived for different Co^{3+} configurations:

Free Co^{3+}	$E_1 = -10K$
Octahedrally surrounded high-spin Co^{3+}	$E_2 = -4Dq - 10K$
Octahedrally surrounded low-spin Co^{3+}	$E_3 = -24Dq - 6K$
Tetrahedrally surrounded high-spin Co^{3+}	$E_4 = -\frac{8}{3}Dq - 10K$

A "critical" Dq value for spin pairing in Co^{3+} is reported to be 2350 cm^{-1} (*38*). Therefore $E_3 - E_2 = -20Dq + 4K = 0$, if Dq equals 2350 cm^{-1}. From this equation a K value of 11750 cm^{-1} or 141 kJ/mol can be derived. From the heat of hydration of Co^{3+} (*47*) an octahedral stabilization energy of Co^{3+}, with respect to the free ion, as 188 kJ/mol is estimated (*44*), so $E_3 - E_1 = -24Dq + 4K = -188$ kJ/mol. Using the K value of 141 kJ/mol the Dq value of Co^{3+} can be calculated to be 31.3 kJ/mol. The octahedral site preference energy of Co^{3+} can be expressed as $E_4 - E_3$, which is equal to $\frac{64}{3}Dq - 4K$. In the above it is shown that $E_3 - E_1 = -24Dq + 4K = -188$ kJ/mol. Therefore $E_4 - E_3 = -\frac{8}{3}Dq + 188 = 105$ kJ/mol, using the Dq value of 31.3 kJ/mol. This result is not very sensitive to the calculated value of K.

(c) *The Relative Octahedral Site Preference Energy of Co^{3+} versus Al^{3+}*

In the above the absolute octahedral site preference energies of Co^{3+} and Al^{3+} have been calculated to be 105 and 62 kJ/mol, respectively. Therefore the relative octahedral site preference energy of Co^{3+} with respect to Al^{3+} is 43 kJ/mol.

ACKNOWLEDGMENTS

This study was supported by the Netherlands Foundation for Chemical Research (SON) with financial aid from the Netherlands Organization for the Advancement of Pure Research (ZWO). Thanks are due to Dr. B. Koch and Mr. W. Molleman (University of Amsterdam) for the XRD measurements, to Mr. A. Terpstra (University of Amsterdam) for the use of the DRS apparatus and to Dr. ir. V. H. J. de Beer (Eindhoven University of Technology) for helpful discussion.

REFERENCES

1. de Beer, V. H. J., van Sint Fiet, T. H. M., van der Steen, G. H. A. M., Zwaga, A. C., and Schuit, G. C. A., *J. Catal.* **35,** 297 (1974).
2. Wivel, C., Candia, R., Clausen, B. S., Mørup, S., and Topsøe, H., *J. Catal.* **68,** 453 (1981).
3. Massoth, F. E., "Advances in Catalysis," Vol. 27, p. 265. Academic Press, New York, 1978.
4. Gates, B. C., Katzer, J. R., and Schuit, G. C. A., "Chemistry of Catalytic Processes," Chap. 5. McGraw–Hill, New York, 1979.
5. Grange, P., *Catal. Rev.* **21,** 135 (1980).
6. Ratnasamy, P., and Sivasanker, S., *Catal. Rev.* **22,** 401 (1980).
7. Delmon, B., *in* "Proceedings, 3rd International Conference on the Chemistry and Uses of Molybdenum" (H. F. Barry and P. C. H. Mitchell, Eds.), p. 73. Climax Molybdenum Co., Ann Arbor, Michigan, 1979.
8. Farragher, A. L., and Cossee, P., *in* "Proceedings, 5th International Congress on Catalysis, Palm Beach, 1972" (J. Hightower, Ed.), p. 1301. North-Holland, Amsterdam, 1973.
9. de Beer, V. H. J., and Schuit, G. C. A., *in* "Preparation of Catalysts" (B. Delmon, P. A. Jacobs, and G. Poncelet, Eds.), p. 343. Elsevier, Amsterdam, 1976.
10. Topsøe, H., Clausen, B. S., Candia, R., Wivel, C., and Mørup, S., *J. Catal.* **68,** 433 (1981).
11. de Beer, V. H. J., Duchet, J. C., and Prins, R., *J. Catal.* **72,** 369 (1981).
12. Duchet, J. C., van Oers, E. M., de Beer, V. H. J., and Prins, R., *J. Catal.* **80,** 386 (1983).
13. Lo Jacono, M., Cimino, A., and Schuit, G. C. A., *Gazz. Chim. Ital.* **103,** 1281 (1973).
14. Tomlinson, J. R., Keeling, R. O., Rymer, G. T., and Bridges, J. M., "Actes du 2me Congr. Int. Catal.," p. 1831. Editions Technip, Paris, 1961.
15. Ashley, J. H., and Mitchell, P. C. H., *J. Chem. Soc. A,* 2730 (1969).
16. Ueda, H., and Todo, N., *J. Catal.* **27,** 281 (1972).
17. Lo Jacono, M., Verbeek, J. L., and Schuit, G. C. A., *J. Catal.* **29,** 463 (1973).
18. Ratnasamy, P., Ramaswamy, A. V., Banerjee, K., Sharma, D. K., and Ray, N., *J. Catal.* **38,** 19 (1975).
19. Grimbolt, J., Bonnelle, J. P., and Beaufils, J. P., *J. Electron Spectrosc. Relat. Phenom.* **8,** 437 (1976).
20. Declerck-Grimée, R. I., Canesson, P., Friedman, R. M., and Fripiat, J. J., *J. Phys. Chem.* **83,** 885 (1978).
21. Topsøe, H., Clausen, B. S., Burriesci, N., Candia, R., and Mørup, S., *in* "Preparation of Catalysts, II" (B. Delmon, P. Grange, P. A. Jacobs, and G. Poncelet, Eds.), p. 479. Elsevier, Amsterdam, 1979.
22. Lycourghiotis, A., Defossé, C., Delannay, F., Lemaitre, J., and Delmon, B., *J. Chem. Soc., Faraday Trans. 1* **76,** 1677 (1980).
23. Greegor, R. B., Lytle, F. W., Chin, R. L., and Hercules, D. M., *J. Phys. Chem.* **85,** 1232 (1981).
24. Chung, K. S., and Massoth, F. E., *J. Catal.* **64,** 320 (1980).
25. Chin, R. L., and Hercules, D. M., *J. Phys. Chem.* **86,** 360 (1982).

26. Chung, K. S., and Massoth, F. E., *J. Catal.* **64,** 332 (1980).
27. Topsøe, N. Y., and Topsøe, H., *J. Catal.* **75,** 354 (1982).
28. Massoth, F. E., and Chung, K. S., *in* "Proceedings, 7th International Congress on Catalysis, Tokyo, 1980" (T. Seiyama and K. Tanabe, Eds.), p. 629. Elsevier, Amsterdam, 1981.
29. Jenkins, J. W., McNicol, B. D., and Robertson, S. D., *CHEMTECH* **7,** 316 (1977).
30. Hurst, N. W., Gentry, S. J., Jones, A., and McNicol, B. D., *Catal. Rev.* **24,** 233 (1982).
31. Thomas, R., van Oers, E. M., de Beer, V. H. J., Medema, J., and Moulijn, J. A., *J. Catal.* **76,** 241 (1982).
32. Klug, H. P., and Alexander, L. E., "X-Ray Diffraction Procedures," p. 491. Wiley, New York, 1954.
33. Arnoldy, P., van Oers, E. M., Bruinsma, O. S. L., de Beer, V. H. J., and Moulijn, J. A., *J. Catal.*, in press.
34. Gentry, S. J., Hurst, N. W., and Jones, A., *J. Chem. Soc., Faraday Trans. 1* **65,** 1688 (1979).
35. Wimmers, O. J., Arnoldy, P., and Moulijn, J. A., submitted for publication.
36. Brown, R., Cooper, M. E., and Whan, D. A., *Appl. Catal.* **3,** 177 (1982).
37. Puxley, D. C., Kitchener, I. J., Komodromos, C., and Parkyns, N. D., *in* "Preparation of Catalysts, III" (G. Poncelet, P. Grange, and P. A. Jacobs, Eds.), p. 237. Elsevier, Amsterdam, 1983.
38. Dunitz, J. D., and Orgel. L. E., *J. Phys. Chem. Solids* **3,** 318 (1957).
39. Kung, H. H., *J. Catal.* **73,** 387 (1982).
40. Arnoldy, P., van den Heijkant, J. A. M., de Bok, G. D., and Moulijn, J. A., *J. Catal.* **92,** 35 (1985).
41. Richardson, J. T., and Vernon, L. W., *J. Phys. Chem.* **62,** 1153 (1958).
42. Knözinger, H., and Ratnasamy, P., *Catal. Rev.* **17,** 31 (1978).
43. John, C. S., Alma, N. C. M., and Hays, G. R., *Appl. Catal.* **6,** 341 (1983).
44. McClure, D. S., *J. Phys. Chem. Solids* **3,** 311 (1957).
45. Navrotsky, A., and Kleppa, O. J., *J. Inorg. Nucl. Chem.* **29,** 2701 (1967).
46. Orgel, L. E., "An Introduction to Transition-Metal Chemistry: Ligand Field Theory," 2nd ed. Methuen, London, 1966.
47. Holmes, O. G., and McClure, D. S., *J. Chem. Phys.* **26,** 1686 (1957).